*Journal of Sound and Vibration* (2001) **240**(4), 679–704
doi:10.1006/jsvi.2000.3263, available online at http://www.idealibrary.com on IDEAL®

# ON THE EIGENFREQUENCIES OF A FLEXIBLE ARM DRIVEN BY A FLEXIBLE SHAFT

O. KOPMAZ† AND K. S. ANDERSON

*Department of Aeronautical Engineering, Mechanical Engineering, and Mechanics, Rensselaer Polytechnic Institute, Troy, NY* 12180-3590, *U.S.A. E-mail: anderk5@rpi.edu*

(*Received* 9 *July* 1999, *and in final form* 20 *July* 2000)

The simulations of multibody dynamic systems with flexible components are generally based on solving the equations of motion by using approximate methods. This approach is taken because these systems' closed-form solutions are often not directly available. These methods often assume a solution as a finite series in terms of modal functions with time-varying coefficients. The eigenmodes of the system under study are preferable as the set of the basis functions used in these series because such expansions provide greater accuracy with fewer terms. As a consequence, accurate estimation of system eigenfrequencies and eigenmodes is extremely useful (potentially necessary) in the effective modelling and simulation of these systems. In this paper, a new general model consisting of rotor, shaft, hub, beam, and payload, as might be encountered in certain industrial robots, is presented and investigated. This model is similar in nature to those studied previously by a number of researchers, but it is more general in form. The authors believe that this model contains a more realistic (and higher fidelity) representation of the rotor–shaft–hub assembly of this system and its interaction with a flexible beam (arm) and associated payload. Through this model the relative influence of seven key dimensionless mass, stiffness and geometric parameters (ratios) on system eigenfrequencies and modes may be qualitatively and quantitatively investigated. These investigations may include many special cases such as flexible shaft + rigid beam, rigid shaft + flexible beam, cantilever–free beam, pinned–free beam, fixed–free shaft, etc. Given the volume of numerical studies which may be performed to this end, this paper concentrates on the effect of the two parameters representing the mass and stiffness ratios of the system manipulator on its driveline.



## 1. INTRODUCTION

Modelling and simulation of multibody dynamic systems has become indispensable in the design and control of such systems. In many situations, these mechanical systems cannot be adequately modelled and their behavior predicted if the flexibility, including flexible body characteristics, of the system components are neglected. This is especially the case for mechanical systems which have highly compliant or large links, and are subjected to high driving torques in order to obtain high operation speeds. In such instances, the behavior (and potentially performance) of the system can be heavily influenced by the link flexibilities. In such cases, system modelling and analysis which includes all the structural flexibility is helpful, if not absolutely necessary. Such modelling requirements may be

† Visiting Professor
Permanent Address: Department of Mechanical Engineering, College of Engineering and Archecture, Uludag University, Bursa 16059, Turkey.

0022-460X/01/090679 + 26 $35.00/0 

unavoidable in order to develop reliable dynamic models which can be used to accurately predict system response through the entire range of operation speeds, and scenarios. Such a dynamic model is also useful in gaining insight into what design parameters most influence specific aspects of the dynamic response of the system, and thus may be modified so to adjust the system behavior in a desired manner. In this way, one may determine which parameters may be modified so to most effectively reduce undesired vibrations. In multibody dynamic analysis of continuous bodies, deflections are usually approximated by using truncated modal expansions. The use of a more accurate (representative) set of basis functions allows for the use of fewer terms in the finite series approximation, without loss of accuracy. In this regard, a more accurate system model will help determine more realistic eigenvalues and eigenmodes, which in turn may be used to produce a more accurate, less complex discrete system model.

The flexibility of the drive train (driving shaft, transmission gears, etc.) of mechanical system often plays an important role in the dynamic behavior of the system, and should be included in the model. Typical examples of these applications are heavily loaded cam and gear mechanisms, mechanical systems driven through long transmission shafts, some spacecraft solar array drive assemblies and deployment mechanisms, and some robot manipulators applications. The system studied in this work is in the form of a motor–shaft–hub–one-ink robot arm–payload assembly, as shown in Figure 1. Through the investigation of this system two principal objectives are pursued. Firstly, this work studies the coupled effects of link and shaft flexibility on the eigenfrequencies of a distributed parameter model (DPM) and compares the results with those of the models in which the driving shaft or transmission line is represented by a torsional spring. This comparison emphasizes the importance of modelling by demonstrating how *significant* variations in predicted behavior of the system can result from "*simple*" differences in the model. The second aim of this work is to determine the exact eigenfrequencies leading to the exact eigenmodes of the system, which may in turn be used to more efficiently and accurate solve the equation of motions by modal expansion.

The DPMs lead to a set of partial differential equations of motion. In general, an exact and closed analytical solution cannot be obtained, thus some approximate solution procedures must be applied. These procedures generally involve some form of model discretization, which reduces the system of equations from a set of generally coupled non-linear partial differential equations (PDEs), to a system of generally coupled non-linear ordinary differential equations (ODEs). One of the most common discretizations used in analytical dynamics is based on truncated (finite) modal expansions. In this regard,

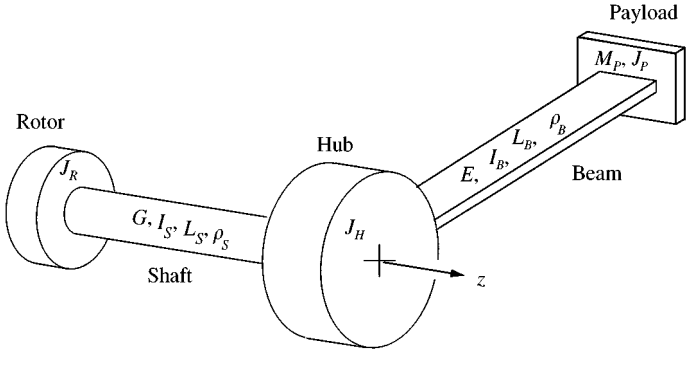


Figure 1. Full distributed system model.

the determination of the highly accurate, if not exact eigenmodes of the system (satisfying as many boundary conditions as possible) is of great importance because it makes it possible to obtain an accurate series solution with a reduced number of terms.

Since the late 1980s research associated with the two main scopes of this work have been carried out. Barbieri and Ozguner [1] in 1988 investigated unconstrained and constrained modal expansions for a rotating link. They concluded that pinned mode shapes are inadequate for the analysis of flexible structures in slewing maneuvers. Furthermore, they found that both the constrained and unconstrained mode expansions are not accurate in the first flexible frequency as far as motor dynamics is not considered. In this work, the authors did not account for joint or shaft flexibility.

Also in 1988, Yigi *et al.* [2] presented results considering a distributed radially rotating beam with a tip mass, connected at the beam root to a rigid body. A set of coupled non-linear equations were derived for the system using the extended Hamilton's principle. The effect of coupling terms upon the vibration waveforms were investigated by using both linearized and numerical solution of the differential equations. The results found that even for small values of the ratio of the flexible beam to rigid-body inertias, the uncoupled equations can lead to substantially incorrect results.

Bellezza *et al.* [3] derived the equations of motion of a rotating beam with a rotating inertia at its base and a concentrated mass at its tip by using two different non-inertial rotating frames. They showed that the frequency equation does not differ because the physical system remains the same. These authors, however, do not consider the shaft or transmission flexibility in general. A more detailed discussion of the resonance conditions of deformable bodies and the use of multiple co-ordinate sets can be found in reference [4]. In his paper, Shabana discusses and explains why the same solutions in multibody simulations can be obtained even if two different sets of mode shapes and two different sets of co-ordinate systems are used. He also emphasizes that the mode shapes and the co-ordinate systems of deformable bodies undergoing large rigid-body displacements cannot be selected arbitrarily.

In 1990, Low [5] analysed the eigenfrequencies of a Bernoulli–Euler beam attached to a compliant, rotating hub. He developed a model in which the hub is connected to the base by lumped torsional and linear springs. Furthermore, he defined some non-dimensional parameter and studied the affects of various combinations including extreme cases (e.g., corresponding to different boundary conditions of beam). The same author [6] later studied the affects of hub inertia and payload on the vibration of a flexible—rotating beam. The author states that the mode shapes are a function of the feedback control and the actual frequencies depend on the motor inertias.

Garcia and Inman [7] presented the formulation of a model for a single-link flexible beam, without end mass or payload, undergoing a slewing maneuver at an actively controlled pinned end. The driveline stiffness (motor, gears, and rotation position feedback constant) was treated as an *equivalent* lumped linear spring, referred to as the "servo stiffness". They showed that for low- to-moderate ratios of the servostiffness to beam stiffness, the treatment of the beam using clamped–free modes leads to an erroneous system model.

Xi and Fenton [8] investigated the coupling effect of a flexible link and a flexible joint in a one-link rotating structure. They defined two non-dimensional parameters (actually two ratios: the ratio of a bending-type stiffness of the link to the torsional stiffness of the rotor-beam joint; and the moment of inertia ratio of the link to the rotor) and compared unconstrained (joint rotation affects link deflection) and constrained (joint rotation does not affect link deflection) modal expansions. That same year, Xi *et al.* [9] studies the same subject but for two special cases, i.e., a manipulator with a relatively flexible link and

a relatively rigid joint; and a second type with the properties contrary to the first. In the last three works, the flexibility of the drive line, whether caused by the driving shaft or by the shaft-to-link joint, is represented by a torsional spring. The detailed information on this modelling in flexible joint robots is found in Potkonjak's paper [10].

In 1996, Morris and Taylor [11], using Hamilton's Principle, developed the equations of motion for a single distributed flexible link, possessing a tip (payload) mass and rotational inertia. The derivation presented in this work is very similar to that in reference [2], but ignores the geometric stiffness effects due to centripetal accelerations which were considered by Yigit *et al.* [2]. This work demonstrated that the model presented by the authors performed better in predicting experimentally determined results than the use of a "classical" model.

The study presented in this paper differs from the aforementioned articles in that the shaft is considered to be a continuous bar performing torsional vibrations. Additionally, the coupled non-linear equations of motion are derived in very general fashion considering the influence of rotor, shaft, hub, beam, and payload, as well as geometric stiffness terms which arise from both centripetal and Coriolis accelerations. Proceeding in this manner, a more complete distributed parameter representation for the system is achieved which is felt by the authors to be a more accurate (and thus exact) representation than the models presented in the aforementioned works.

## 2. A COMPARATIVE MODEL STUDY

In this section, to emphasize the significance of careful (more high fidelity) modelling, a comparison between a discrete parameter model (DcPM) and a DPM representations of the same mechanical system is given. Consider the system shown in Figure 1 letting $J_D$ be the rotational inertia of a *lumped rigid disc* representing the hub, beam and payload which is driven by the flexible shaft. $\rho_s$, $G$, $I_s$, $A_s$ and $L_s$ indicates the density/length, the shear modulus, the polar second area moment, the cross-sectional area and the length of shaft respectively. This is an unconstrained system with regard to rotational motion around the $z$-axis and it may be modelled in two different forms. The first of these forms is a DPM in which the shaft has both distributed mass and distributed flexibility. In the second model the flexibility of the shaft is replaced with a lumped torsional spring and an effective polar inertia of the shaft is at one end of the spring. With $\mu$ being defined as the ratio of the shaft inertia $J_s$ to that of the load (i.e., the lumped disc) $J_D$, the first exact frequency $\lambda_1$, its approximation $\tilde{\lambda}$ from equation (A.12) and its percentage error are given in Table 1. From this table, it is observed that the percentage error between $\lambda_1$ and $\tilde{\lambda}$ tends to zero for $\mu = \sim 6...7$, but increases quickly to $> 10\%$ for $\mu < 5$ or $\mu > \sim 9$. Thus, even between very simplified models, the use of lumped inertia and stiffness representations can give very erroneous results.

## 3. A MORE EXACT DPM

The system model proposed in this work is the full system shown in Figure 1. In this model the shaft is treated as a continuum connected to a rotor inertia, and is considered separately from the distributed beam with lumped payload model, which are in turn coupled through boundary conditions at the hub. Similar models has been used by other authors [2–5, 8, 11, 13] in order to obtain the eigenfrequencies and eigenmodes of the system, which in turn maybe used as basis functions in a finite series for describing the

TABLE 1

*$\lambda_1$ (DPM) and $\lambda$ (DcPM) values for different $\mu$ ratios*

| $\mu$ | $\lambda_1$ | $\lambda$ | Error $= [(\lambda_1 - \tilde{\lambda})/\lambda_1]$ 100% |
|---|---|---|---|
| 0·1 | 1·632 | 1·049 | 36 |
| 0·2 | 1·689 | 1·095 | 35 |
| 0·4 | 1·791 | 1·183 | 34 |
| 0·6 | 1·879 | 1·265 | 33 |
| 0·8 | 1·959 | 1·342 | 31 |
| 1 | 2·029 | 1·414 | 30 |
| 2 | 2·289 | 1·732 | 24 |
| 5 | 2·654 | 2·449 | 8 |
| 10 | 2·863 | 3·317 | − 16 |
| 15 | 2·948 | 4·000 | − 36 |
| 20 | 2·993 | 4·583 | − 53 |
| 25 | 3·021 | 5·099 | − 69 |

forced motion of the arm. Here, as a logical first step, we wish to confine our attention to study the planar motion of the system, but otherwise the initial equations of motion derived are very general in form with few simplifying assumptions.

The system most generally consists of five parts: rotor, shaft, hub, beam, and payload. In most of the papers related to the subject, the hub inertia and hub radius are neglected for the sake of simplicity. In other works, the payload is neglected (applicable for helicopter blades, and many terrestrial manufacturing applications). In this derivation, the individual contributions of the rotor, shaft, hub, arm and payload will all be considered.

## 4. EQUATIONS OF MOTION

For this system there are actually two equations of motion, which are coupled via subsystem boundary conditions (BCs). The first of these represents the subsystem of the rotor (motor armature, etc.) and shaft (driveline exclusive of motor and hub), while the second represents the subsystem of the beam and payload (end effector plus workpiece). These coupling subsystem BCs can be viewed as the equations describing the orientation of the hub, which must be common to the equations of motion associated with each of these subsystems. Figure 2 shows the reference frame, co-ordinate system, and basis vectors associated with the hub–beam–payload subsystem, and with which the elastic deformations of the beam are represented. The reference frame is fixed in the hub at the root of the beam and is oriented such that the local $x$-axis of this rotating frame coincides with the undeformed centerline of the beam.

The details related to the development of the equations of motion and to the derivation of the eigenvalue (frequency) equation is given in Appendix B. In order to generalize the results and aid in their comparison with those of other works, the follwing non-dimensional parameter are introduced:

$$R_a := \frac{\frac{1}{3}\rho_B A L_B^3}{J_R} = \frac{J_B}{J_R}, \qquad R_b := \frac{EI_B/L_B}{GI_s/L_s}, \tag{1, 2}$$

$$R_c := \frac{\frac{1}{3}\rho_B A L_B^3}{\rho_s I_s L_s} = \frac{J_B}{J_s}, \qquad R_d := \frac{\frac{1}{3}\rho_B A L_B^3}{J_H} = \frac{J_B}{J_H}, \tag{3, 4}$$

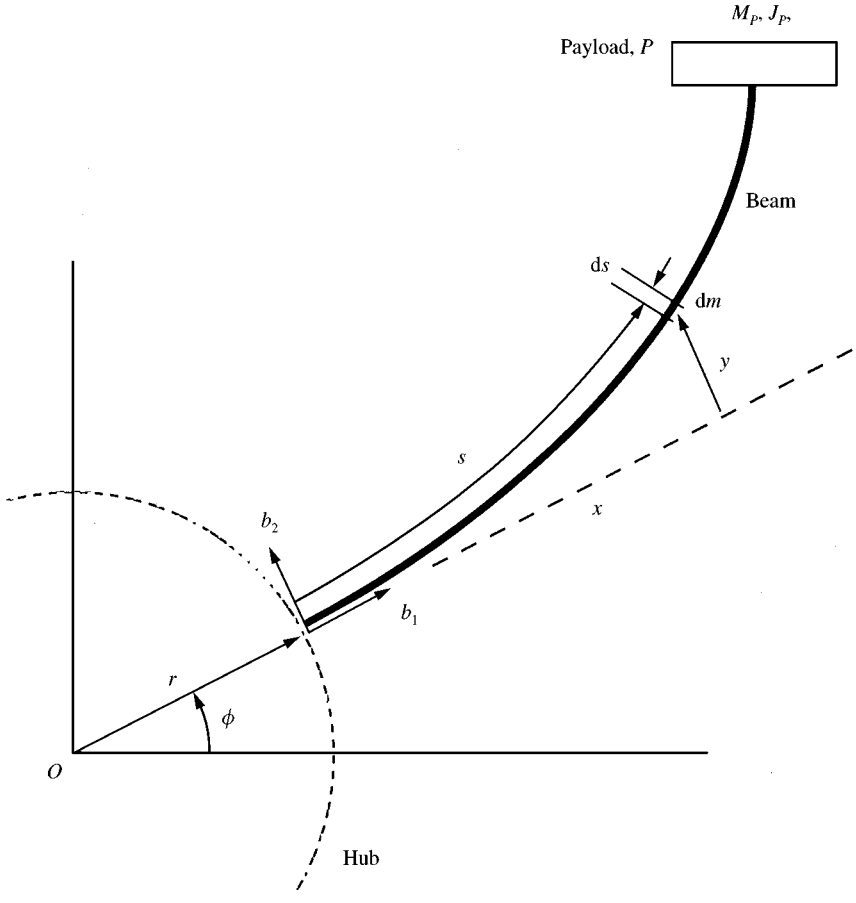


Figure 2. Local beam reference frame and co-ordinate system.

$$R_e := \frac{J_P}{3J_B}, \qquad R_f := \frac{M_P}{M_B}, \qquad \alpha := \frac{1}{3}\frac{R_b}{R_a}, \tag{5–7}$$

$$\beta := \frac{1}{3}\frac{R_b}{R_c}, \qquad \gamma := \frac{1}{3}\frac{R_b}{R_d}, \qquad \bar{r} := \frac{r}{L_B}, \tag{8–10}$$

where $A_B$ represents the cross-sectional area of the beam, $E$ represent the Young's modulus of the beam material, $I_B$ is the area moments of inertia of the beam, $J_B$, $J_H$, $J_P$, $J_R$ are the rigid-body mass moment of inertias of the beam about its root, the hub, payload, and rotor, respectively, $L_B$ is the length of the beam, $M_B$, $M_P$ are the masses of the beam and payload, $\rho_B$, $\rho_s$ are the mass densities of the beam and shaft, respectively, and $r$ is the hub radius.

The system, characteristic determinant, in terms of the above-mentioned parameters, which leads to the eigenvalue (frequency) equation is given by equation (B.48) in Appendix B, but its expansion is not given here due to its complexity. However, the determinant given by equation (B.48) can be expanded by using any symbolic mathematical code (e.g., Maple or Mathematica) as has been done for this study.

## 5. TWO SPECIAL CASES

In this section, the two special cases of the model presented in sections 3 and 4 are given. These are the special cases of a flexible shaft–rigid beam system, and a rigid shaft–flexible beam system, and represent limiting cases of $R_b \to \infty$ and $R_b \to 0$, respectively, for which closed-form solutions exist.

### 5.1. FLEXIBLE SHAFT-RIGID BEAM

For this special (limiting) case, the system can be considered as shown in Figure 1, where the beam is now treated is rigid. Here $\tilde{J}$ is equal to the summation of the hub moment of inertia $J_H$, and the quantities $J_B^*$, and $J_P^*$, respectively, represent the beam and payload mass moments of inertia, each with respect to the rotation axis of the shaft. After some simple calculus these quantities are found as

$$J_B^* = (1 + 3\bar{r} + 3\bar{r}^2)\, J_B \tag{11}$$

and

$$J_P^* = J_P + (1 + 2\bar{r} + \bar{r}^2)\, M_P L_B^2. \tag{12}$$

Hence,

$$\tilde{J} = J_H + J_B^* + J_P^* = J_H + (1 + 3\bar{r} + 3\bar{r}^2)\, J_B + [J_P + (1 + 2\bar{r} + \bar{r}^2) M_P L_B^2]. \tag{13}$$

The frequency equation of this now degenerate system is associated with a uniform shaft which has two independent rotary inertias at each of its free ends, and performs torsional vibrations as was discussed previously in section 2 (detailed in Appendix A) and is given as

$$\eta^2\, [(\mu_1 \mu_2 \eta^2 - 1) \sin \eta - (\mu_1 + \mu_2)\eta \cos \eta] = 0, \tag{14}$$

where $\mu_1$ and $\mu_2$ are the inertia ratios defined as

$$\mu_1 = \frac{J_R}{J_s} = \frac{J_R/J_B}{J_s/J_B} = \frac{1/R_a}{1/R_c} = \frac{R_c}{R_a} \tag{15}$$

and

$$\mu_2 = \frac{\tilde{J}}{J_s} = \frac{J_H}{J_s} + (1 + 3\bar{r} + 3\bar{r}^2)\, \frac{J_B}{J_s} + \frac{J_P}{J_s} + (1 + 2\bar{r} + \bar{r}^2)\, \frac{M_P L_B^2}{J_s}$$

$$= \frac{J_H}{J_B}\, \frac{J_B}{J_s} + (1 + 3\bar{r} + 3\bar{r}^2)\, \frac{J_B}{J_s} + \frac{J_P}{J_B}\, \frac{J_B}{J_s} + (1 + 2\bar{r} + \bar{r}^2)\, \frac{M_P L_B^2}{(\frac{1}{3} M_B\ L_B^2)}\, \frac{J_B}{J_s}$$

or

$$\mu_2 = \frac{\tilde{J}}{J_s} = \left[\frac{1}{R_d} + (1 + 3\bar{r} + 3\bar{r}^2) + 3R_e + 3\,(1 + 2\bar{r} + \bar{r}^2)\, R_f\right] R_c \tag{16}$$

with $\eta$ defined as

$$\eta = \omega\, \frac{L_s}{\tilde{c}}. \tag{17}$$

TABLE 2

*The eigenvalues obtained by equations* (61) *and* (64) ($R_a = 1, R_b = 10^7, R_c = R_d = 10^4, \bar{r} = 0$); conversion factor $\sqrt{\beta} = 18{\cdot}2574$

| $\lambda$ equation (B.48) | $\sqrt{\beta}\,\lambda^2$ equation (18) | $\eta$ equation (14) |
|---|---|---|
| 0·0278 | 0·0141 | 0·0141 |
| 0·4148 | 3·1417 | 3·1417 |
| 0·5866 | 6·2832 | 6·2832 |
| 0·7185 | 9·4248 | 9·4248 |
| 0·8296 | 12·5664 | 12·5664 |
| 0·9276 | 15·7080 | 15·7080 |

This case corresponds to the limiting case $R_b \to \infty$. In the case of $\mu_1 = 0$ and/or $\mu_2 = 0$, equation (14) is the frequency equation of a free–free uniform bar with an inertia at one end [9]. In our exact model, this case can be approached for $R_b \geqslant 10^6$. For the parameter values $R_b = 10^6$, $R_a = 1$, $R_c = R_d = 10^3$, $R_e = R_f = \bar{r} = 0$, the system eigenvalues $\lambda$ and $\eta$ as obtained from equations (B.48) and (14), respectively, are listed in Table 2. Except at the true limits represented by these special cases, the relationship

$$\eta = \sqrt{\beta}\lambda^2 \tag{18}$$

exists between $\lambda$ and $\eta$, which arises because these two quantities are related to each other via $\omega$.

### 5.2. RIGID SHAFT–FLEXIBLE BEAM

For this special case representing $R_b = 0$, the system can be considered as a *pinned–free* flexible beam with inertias fixed at the beam's ends. Here, $\tilde{J}$ includes $J_R$, $J_s$ and $J_H$ such that

$$\tilde{J} = J_R + J_s + J_H. \tag{19}$$

The frequency (or eigenvalue) equation is found to be

$$\begin{aligned}
&\lambda^2\,[2\lambda\,(\bar{r} + R_f - \lambda^4 R_e \bar{r}(R_f + \bar{r}))\sinh\lambda\sin\lambda + 2(-1 + \lambda^2\bar{r}(\bar{r} + 2R_f)\\
&\quad + \lambda^4 R_e(R_f + 2\bar{r} - \lambda^2 R_f\bar{r}^2))\sinh\lambda\cos\lambda + (1 - \lambda^2\bar{r}(\bar{r} + 2R_f)\\
&\quad + \lambda^4 R_e(R_f + 2\bar{r} - \lambda^2 R_f\bar{r}^2))\cosh\lambda\,\sin\lambda\, + 2\lambda^3\,(R_e + R_f\bar{r}^2)\cosh\lambda\cos\lambda\\
&\quad + \mu\,(\lambda^3\,[(1 + \lambda^4 R_e R_f) + (1 - \lambda^4 R_e R_f)\cosh\lambda\cos\lambda]\\
&\quad + \lambda^4\,[-(R_f + \lambda^2 R_e)\cosh\lambda\cos\lambda + (R_f - \lambda^2 R_e)\cosh\lambda\,\sin\lambda])] = 0,
\end{aligned} \tag{20}$$

where

$$\mu = \frac{\tilde{J}}{J_B} = \frac{J_R + J_s + J_H}{J_B} = \frac{J_R}{J_B} + \frac{J_s}{J_B} + \frac{J_H}{J_B} = \frac{1}{R_a} + \frac{1}{R_c} + \frac{1}{R_d}. \tag{21}$$

For $R_a = \bar{r} = R_e = R_f = 0$, equation (20) gives the frequency equation derived in reference [8]. For the case where we additionally have $\mu = 0$, equation (20) is the same as that of a pinned–free beam. When $\mu \to \infty$, equation (20) transforms into the frequency equation of a cantilever beam provided that all the terms must be divided by $\mu$ before $\mu$ goes to infinity [12]. This case can be approximated with equation (B.48) by taking $R_b$ sufficiently small such that $R_b \leqslant 10^{-6}$.

Note that the frequency equations related to these extreme (limiting) cases cannot be obtained from equation (B.48) by the simple substitutions $R_b \to \infty$ or $R_b = 0$, because there are two different continuous media in the model. However, the frequency equations of these cases can be obtained from equations (B.32) to (B.41) by considering that $A$ and $B$ must be zero for $R_b = 0$, and similarly $a, b, c, d = 0$ for $R_b \to \infty$.

## 6. NUMERICAL RESULTS AND DISCUSSION

The frequency equation of the model presented in this work includes seven dimensionless parameters: $R_a$, $R_b$, $R_c$, $R_d$, $R_e$, $R_f$, and $\bar{r}$. $R_a$, $R_c$, $R_d$, $R_e$, and $R_f$, are inertial ratios, $R_b$ is a stiffness ratio, and $\bar{r}$ is a geometric ratio. Through the resulting frequency equation (from equations (B. 48)) it is possible through numerical studies to determine how each parameter individually affects the eigenfrequencies. However, due to the incredible volume of possible parameter value combinations that a thorough treatment of all seven parameters presents, the authors have chosen to limit the results presented in this paper to the parameters $R_a$ and $R_b$. The influence of payload inertia ratios, $R_e$, $R_f$, as well as prescribed shaft input rotation rate $\dot{\varphi}(0, t)$, are the topics of on going work.

### 6.1. EFFECT OF $R_a$

$R_a$ is the ratio of the moment of inertia of the beam to that of the rotor, exclusive of the shaft. A decrease in $R_a$ means that either the beam inertia decreases or the rotor inertia increases, i.e., a shift towards the case of a cantilever beam. It is reported in reference [1] that $R_a$ affects the frequencies and mode shapes of a system with a flexible link and rigid joint. For this reason, four cases representing a wide range of $R_b$ values (spanning 3 orders of magnitude) were simulated to investigate the effect of $R_a$ on the system frequencies. Figures 3(a–d), show the variation of the first four eigenvalues, respectively, associated with all four $R_b$ values considered. By comparison, Figures 4(a–d) show the variations of the first five eigenfrequencies as a function of $R_a$, for each of the four chosen values of $R_b$ respectively.

Figures 3(a–d) indicate that in all cases the eigenfrequencies remain approximately constant with $R_a$ or increase only modestly in the first frequency. From inspection of Figures 3(a–d) one concludes that the fundamental frequency is most sensitive to $R_a$. Increasing $R_a$ over the range of $0 \to \infty$ for a set $R_b$ value represents a transition of the system from a pinned–free beam, with a spring opposing rotation of the beam at the pinned end, to a pinned–free beam with no such spring. When $R_b$ becomes larger the effect of $R_a$ diminishes for all frequencies. Figure 3(b) shows the variation of the second frequency versus $R_a$. For the cases of $R_b > 1$ this frequency remains almost constant. A similar behavior is also observed for the third eigen for $R_b > 0{\cdot}1$, as indicated in Figure 3(c). Within the range of $R_b$ considered, the fourth and higher eigenfrequencies remain unchanged irrespective of $R_a$; Figure 3(d). Figures 4(a–d) demonstrate how the first five frequencies vary on $R_a$ for constant $R_b$. In all these figures it is observed that only the first frequency varies

prominently with variations in $R_a$, with the second eigenvalue varying almost indistinguishably, and all higher eigenvalues remaining effectively constant.

Another interesting point to be mentioned is the decrease in all frequencies as $R_b$ increases. An increase in $R_b$ corresponds to either an increase in the beam stiffness, a decrease in the shaft stiffness, or a combination thereof. In any regard, an increasing $R_b$ can be interpreted that the shaft is becoming more flexible relative to the beam. Thus, it is clear that the shaft plays a determining role in the formation of low frequencies. A similar situation is observed in the graphics given in reference [7].

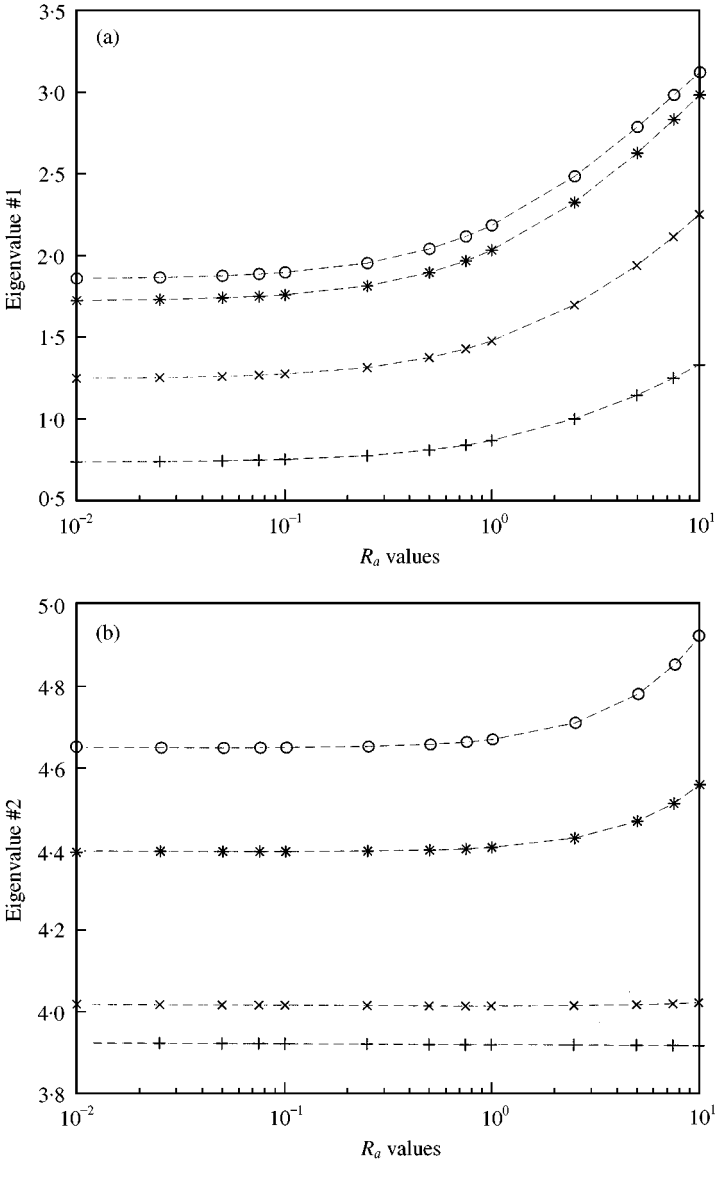


Figure 3. Variation of each of the first four eigenvalues with $R_a$ for fixed $R_b$ values: ○, $R_b = 0{\cdot}01$; *, $R_b = 0{\cdot}1$; ×, $R_b = 1$; +, $R_b = 10$. ($R_c = R_d = 1000$, $\bar{r} = 0{\cdot}001$.) (a) Eigenvalue #1, (b) #2, (c) #3, (d) #4.

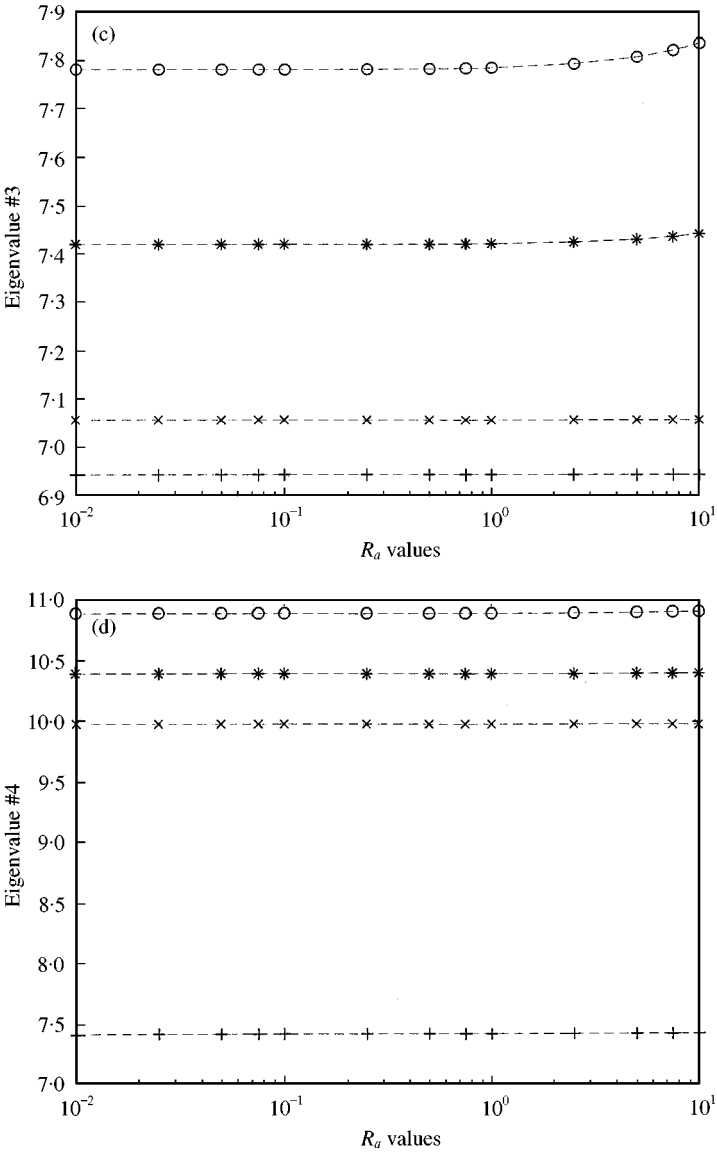


Figure 3. Continued.

It should be remembered that an increase in $R_b$ can be achieved in a variety of ways (e.g., through the variations of $E$, $G$, $I_B$, $I_s$, $L_B$ and $L_s$). For instance, provided that all the other parameters within the definition of $R_b$ are held constant, making the length of the beam smaller yields a larger $EI/L$ ratio, and consequently a large value for $R_b$. But this length variation also has an effect on the other inertial parameters, because of $J_b$. For example, a decrease of 5% in the beam length leads to a decrease of 14% in the beam inertia, which causes variations of the same percentage in the $R_a$, $R_c$, $R_d$, $R_e$, and $R_f$ parameters. Therefore, one has to be careful when making such considerations. In a similar way, some care should be exercised when considering the parameters $\bar{r}$ and $R_d$ because these two ratios include quantities associated with the hub.

### 6.2. EFFECT OF $R_b$

$R_b$ is the ratio of a form of beam stiffness to that of the torsional stiffness of the shaft. Here, the shaft stiffness is defined as the equivalent stiffness of a uniform circular cross-section shaft, i.e., $GI_p/L_s$. Figures 5(a–d) demonstrate how $R_b$ affects the eigenfrequencies for four different $R_a$ values. Here it is observed that all eigenfrequencies decrease as $R_b$ increases. One may view the increase in $R_b$ as a decrease in the shaft stiffness relative to the beam stiffness. If all other quantities are held constant, this would result in a drop in the shaft

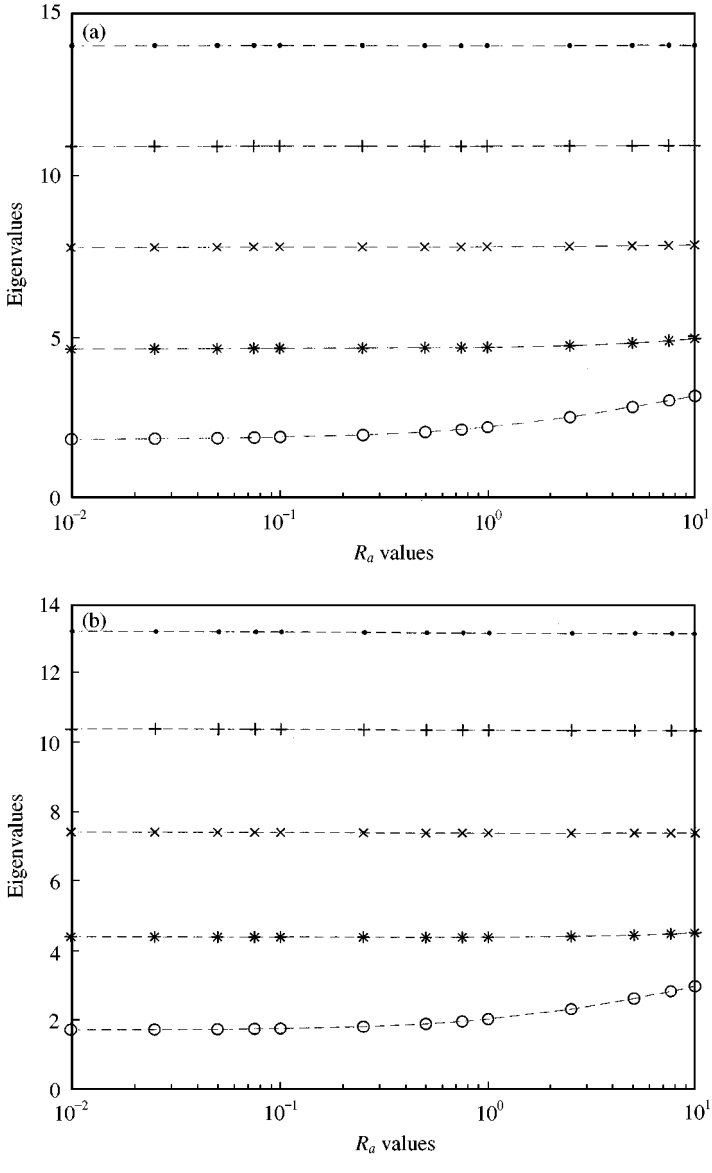


Figure 4. Variation of the first five eigenvalues with $R_a$ for different $R_b$ constants: ○, eigenvalue #1; *, eigenvalue #2; ×, eigenvalue #3; +, eigenvalue #4; ●, eigenvalue #5. ($R_c = R_d = 1000$, $\bar{r} = 0{\cdot}001$.) (a) $R_b = 0{\cdot}01$, (b) 0·10, (c) 1·0, (d) 10·0.

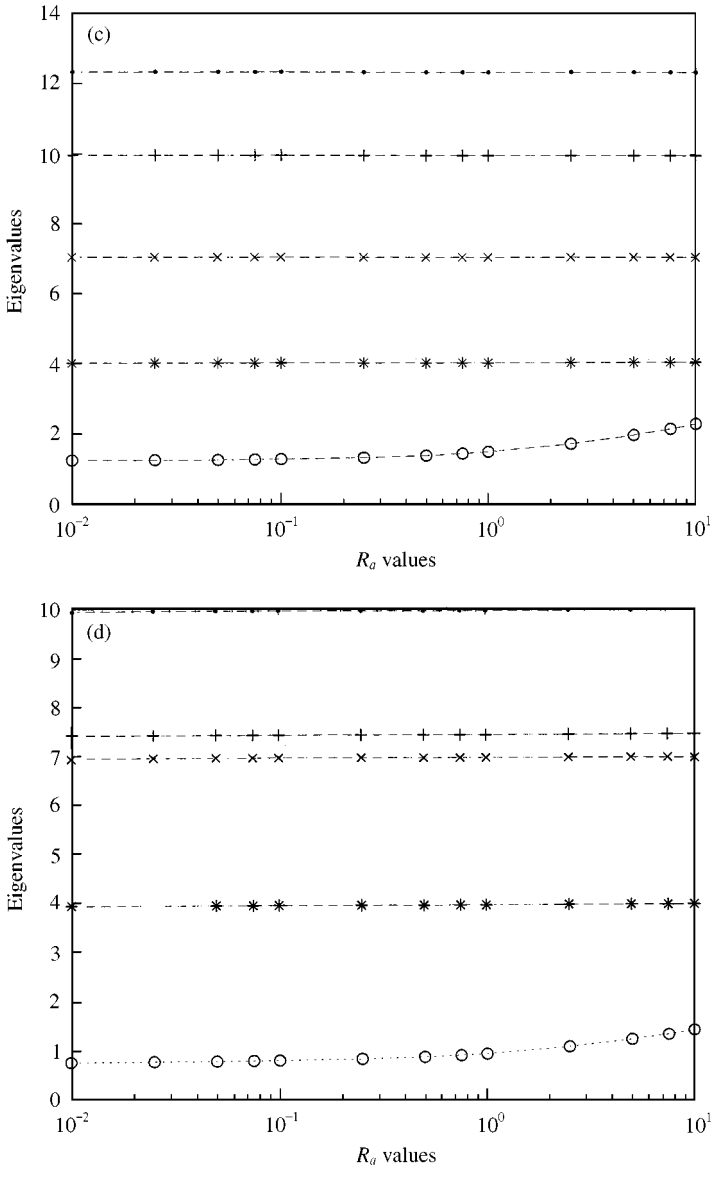


Figure 4. Continued.

torsional modes with an increase in $R_b$. This decrease in eigenfrequencies with increases in $R_b$ is shown in Figures 5(a–d).

The effect of $R_a$ is most significant in the fundamental mode and decrease with both increasing mode number and $R_b$, becoming negligible for modes four and higher. When $R_a$ increases so do all frequencies, again with the effect being negligible for all modes higher than three.

Figures 6(a–d) show how all these frequencies behave for given changes in $R_b$ and constant $R_a$. A general decrease for all frequencies is observed, as has been pointed out earlier, but a more interesting observation may be made from these figures. Specifically, drastic decreases in the fourth and fifth frequencies can be seen with a existence of

a well-defined elbow. This result represents a curve veering phenomenon, as discussed in detail by Perkins and Mote [13]. In that work the authors showed that a curve veer, as opposed to a cross, could result as an artifact of a discretization procedure used in the problem, or solution approximation method such as a perturbation approach. In this work, this curve veering is not caused by any numerical problems because no discretization procedure or perturbation technique has been applied to obtain the frequencies, as it is emphasized in that paper [13]. Therefore, this curve veering represents an actual event or crossing of modes. Specifically, after the veering region the eigenmode shapes associated

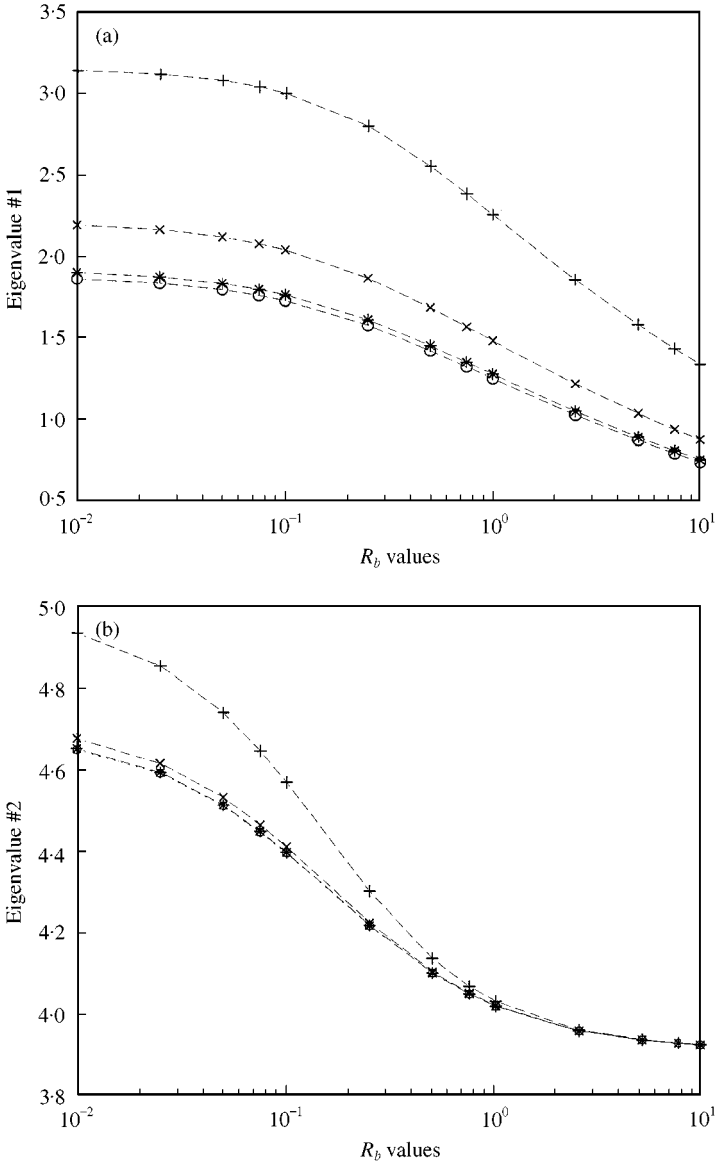


Figure 5. Variation of each of the first four eigenvalues with $R_b$ for fixed $R_a$ values: ○, $R_a = 0{\cdot}01$; *, $R_a = 0{\cdot}1$; ×, $R_a = 1$; +, $R_a = 10$. ($R_c = R_d = 1000$, $\bar{r} = 0{\cdot}001$.) (a) Eigenvalue #1, (b) #2, (c) #3, (d) #4.

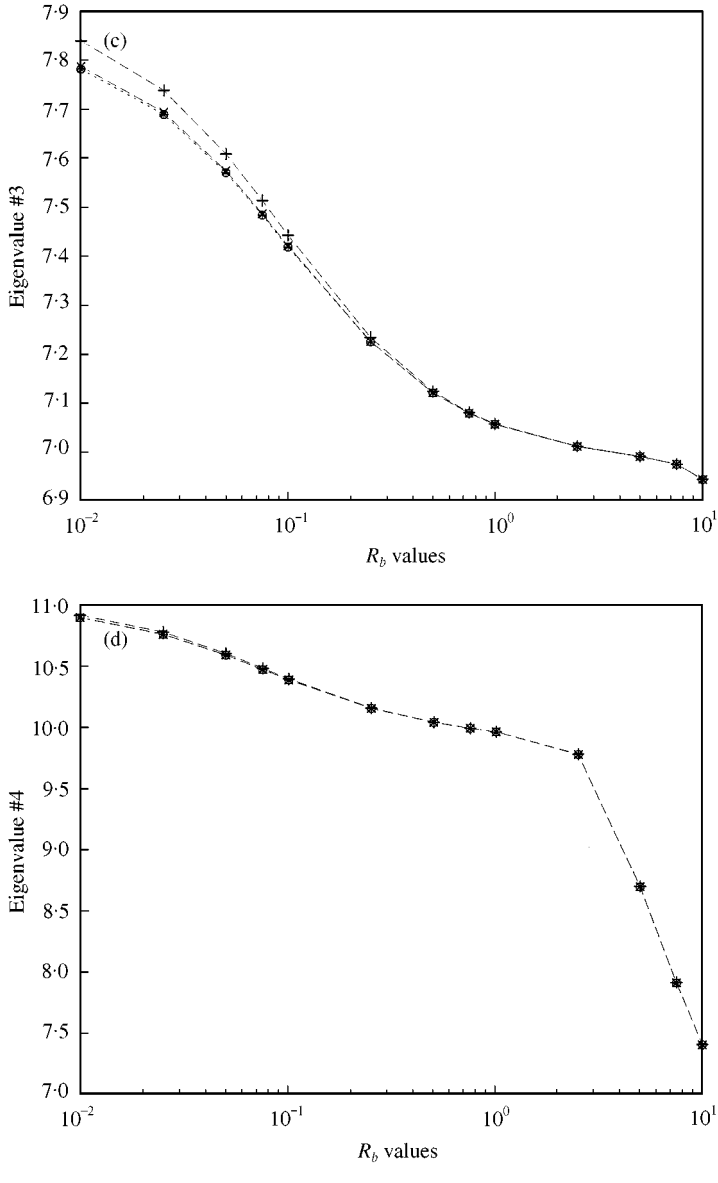


Figure 5. Continued.

with these frequencies interchange. This phenomenon cannot be observed in reference [8] because only the first three frequencies were studied there.

When one compares Figures 3(a–d) and 5(a–d) of this paper with the results given in reference [8], significant differences are obvious. For example, a jump phenomenon of the frequency curves does not appear in the graphics obtained in reference [8]. Moreover, the frequency equation given in reference [8] does not yield the frequencies listed in Tables 2 and 3 of that article, indicating some form of error on the part of that article. By comparison, the model presented within this work is felt to be more exact than the models which are associated with related systems and have previously appeared in the relevant literature. The frequency equation as derived in this work from equation (B.48) is very

general in scope, satisfies limit cases which have been checked against independently obtained results of other authors, and gives reasonable and reliable results overall.

### 6.3. COMMENTS REGARDING $R_c$, $R_d$, $R_e$, $R_f$, $\bar{r}$, AND $\dot{\phi}$

In the results presented in the preceeding sections of this paper, the effects of $R_a$ (and $R_b$) for different values of $R_b$ (and $R_a$) with the values of $R_c$, $R_d$, $R_e$, $R_f$, $\bar{r}$ held

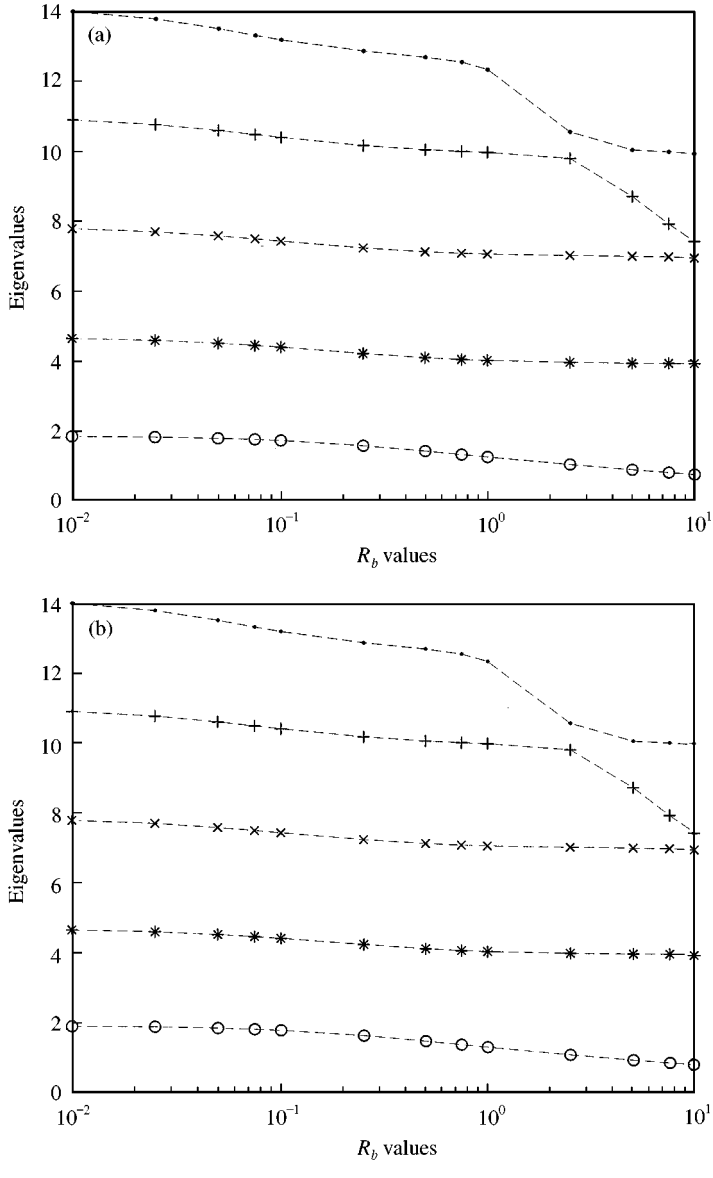


Figure 6. Variation of the first five eigenvalues with $R_b$ for different $R_a$ constants: ○, eigenvalue #1; *, eigenvalue #2; ×, eigenvalues #3; +, eigenvalue #4; ●, eigenvalue #5. ($R_c = R_d = 1000$, $\bar{r} = 0{\cdot}001$.) (a) $R_a = 0{\cdot}01$, (b) 0·10, (c) 1·0, (d) 10·0.

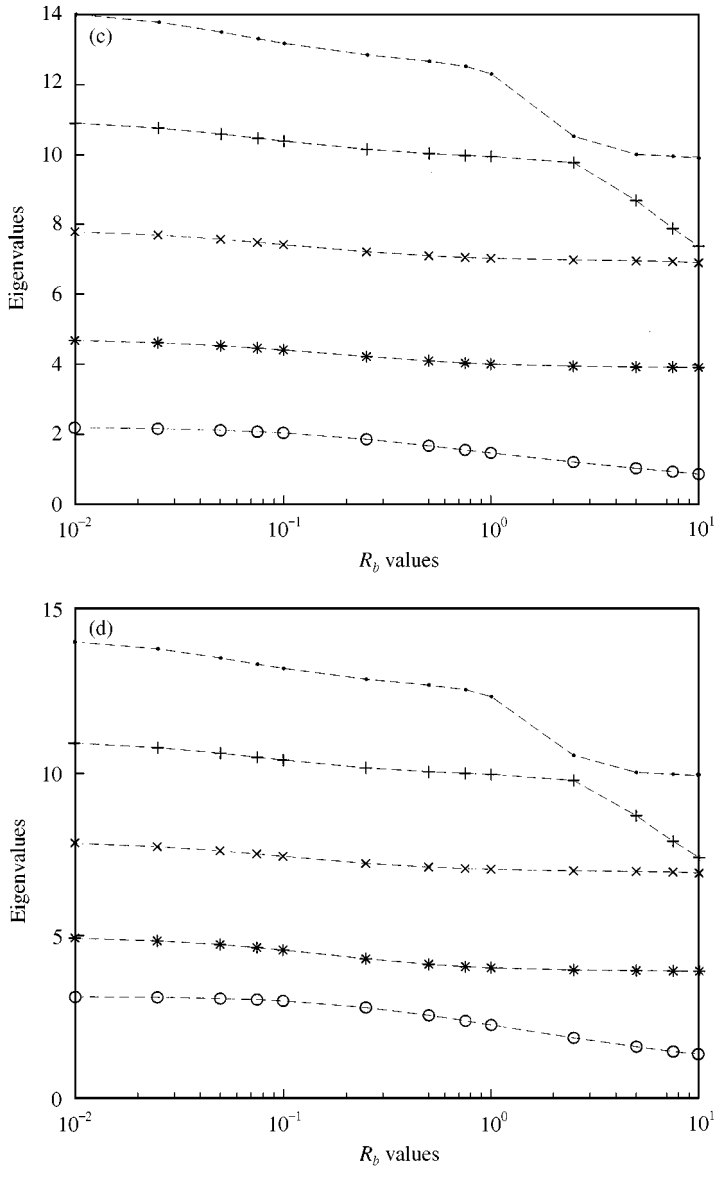


Figure 6. Continued.

constant, and $\dot{\phi}$ neglected, were investigated. To aid in the comparison of these results with those obtained by other investigators, the parameter values of $R_c = R_d = 10^3$, $R_e = R_f = 0$, $\bar{r} = 10^{-3}$, and $\dot{\phi} \cong 0$ were used. These parameter values represent a system with negligible shaft, hub and payload inertias, as well as negligible stiffening (softening) effects arising from centripetal and Coriolis accelerations. It should be noted that the effect of these parameters on the system eigenvalues and associated mode shapes are not in general negligible. Indeed, preliminary work indicates that these parameters (individually, and in combination) can significantly alter the dynamic behavior of the system. This is clearly demonstrated by the results shown in Tables 3–5, which indicate how the first four eigenvalues can be influenced by changes in the dimensionless parameters $R_c$, $R_d$ and $\bar{r}$ respectively. Thus, the particular simplifying assumptions used in modelling the dynamic characteristics of the system need to

TABLE 3

*The first four eigenvalues for various $R_c$ values ($R_a = 0{\cdot}3$, $R_b = 0{\cdot}1$, $R_d = 3$, $\bar{r} = 0$)*

| $R_c$ | $\lambda_1$ | $\lambda_2$ | $\lambda_3$ | $\lambda_4$ |
|---|---|---|---|---|
| $10^{-6}$ | 0·2272 | 0·2624 | 0·2933 | 0·3213 |
| $10^{-3}$ | 0·7358 | 1·0405 | 1·2743 | 1·4711 |
| $10^{-2}$ | 1·2784 | 1·7737 | 1·9196 | 2·2440 |
| $10^{-1}$ | 1·7628 | 2·1638 | 2·9854 | 3·7120 |
| 1 | 1·8215 | 2·9002 | 4·4882 | 4·8993 |

TABLE 4

*The first four eigenvalues for various $R_d$ values ($R_a = 0{\cdot}3$, $R_b = 0{\cdot}1$, $R_c = 1$, $\bar{r} = 0$)*

| $R_d$ | $\lambda_1$ | $\lambda_2$ | $\lambda_3$ | $\lambda_4$ |
|---|---|---|---|---|
| $10^{-3}$ | 1·6922 | 1·8757 | 4·2090 | 4·6941 |
| $10^{-2}$ | 1·7066 | 1·8811 | 4·2107 | 4·6946 |
| $10^{-1}$ | 1·7831 | 1·9675 | 4·2280 | 4·6989 |
| 1 | 1·8191 | 2·5620 | 4·3636 | 4·7523 |
| 10 | 1·8223 | 3·1053 | 4·5500 | 5·1228 |
| 100 | 1·8226 | 3·2029 | 4·5706 | 5·2743 |
| 1000 | 1·8226 | 3·2132 | 4·5725 | 5·2907 |

TABLE 5

*The first four eigenvalues for various $\bar{r}$ values ($R_a = 0{\cdot}3$, $R_b = 0{\cdot}1$, $R_c = 1$, $R_d = 3$)*

| $\bar{r}$ | $\lambda_1$ | $\lambda_2$ | $\lambda_3$ | $\lambda_4$ |
|---|---|---|---|---|
| 0·001 | 1·8287 | 2·8923 | 4·5185 | 4·8421 |
| 0·01 | 1·8280 | 2·8932 | 4·5156 | 4·8469 |
| 0·1 | 1·8215 | 2·9002 | 4·4882 | 4·8933 |
| 0·2 | 1·8143 | 2·9032 | 4·4615 | 4·9411 |
| 0·3 | 1·8073 | 2·9018 | 4·4378 | 4·9857 |
| 0·4 | 1·8005 | 2·8968 | 4·4166 | 5·0272 |
| 0·5 | 1·7941 | 2·8887 | 4·3976 | 5·0658 |
| 0·8 | 1·7765 | 2·8526 | 4·3514 | 5·1656 |
| 1 | 1·7664 | 2·8233 | 4·3280 | |

be very carefully chosen so that the resulting model is not unduly complicated, yet is sufficiently accurate to capture all important characteristics of the system.

## 7. SUMMARY AND CONCLUSIONS

A study has been made of the eigenfrequencies of a distributed rotor–shaft–beam system. The fully coupled, non-linear governing equations are derived for a general distributed parameter model which considers the contributions of rotor, hub, and payload inertias. Additionally, the contribution of geometric stiffening (softening) due to centripetal and Coriolis accelerations are included. It is shown that variations in the ratios of system beam inertia to rotor inertia, and beam stiffness to shaft stiffness, can significantly affect the system fundamental frequency and the associated mode shapes. Moreover, it is

demonstrated that a model considering the distributed nature of both the shaft and beam are necessary if one wishes to accurately predict the system eigenfrequencies. Finally, the affects of hub, shaft, and payload inertia, as well as hub rotation rate may contribute significantly to system behavior, and thus must be considered in the modelling.

## REFERENCES


1. E. Barbieri and U. Ozguner 1988 *Journal of Dynamic Systems, Measurement, and Control* **110**, 416–421. Unconstrained and constrained mode expansions for a flexible slewing beam.
2. A. Yigit, A. Scott and A. G. Ulsoy 1988 *Journal of Sound and Vibrations* **121**, 201–210. Flexible motion of a radially rotating beam attached to a rigid body.
3. F. Bellezza, L. Lanari and G. Ulivi 1990 *Proceedings of IEEE Conference on Robot Automation*. 734–739. Exact modeling of the flexible slewing link.
4. A. A. Shabana 1996 *Journal of Sound and Vibration* **192**, 389–398. Resonance conditions and deformable body coordinate systems.
5. K. H. Low 1990 *Journal of Vibration and Acoustics* **112**, 497–500. Eigen-analysis of a tip loaded beam attracted to a rotating joint.
6. K. H. Low 1997 *Journal of Sound and Vibration* **204**, 823–828. A note on the effect of hub inertia and payload on the vibration of a flexible slewing link.
7. E. Garcia and D. Inman 1991 *American Institute of Aeronautics and Astronautics Journal of Guidance* **14**, 736–743. Modeling of the slewing control of a flexible structure.
8. F. Xi and R. G. Fenton 1994 *International Journal of Robotics Research* **13**, 443–453. Coupling effect of a flexible link and a flexible joint.
9. F. Xi, R. G. Fenton and B. Tabarrok 1994 *Journal of Dynamic Systems, Measurement, and Control* **116**, 826–831. Coupling effects in a manipulator with both a flexible link and joint.
10. V. Potkonjak 1988 *Robotica* **6**, 63–69. Contribution to the dynamics and control of robots having elastic transmissions.
11. K. A. Morris and K. J. Taylor 1996 *SIAM Review* **38**, 294–305. A variational calculus approach to the modelling of flexible manipulators.
12. A. A. Shabana 1997 *Vibration of Discrete and Continuous Systems*. New York: Springer: first edition.
13. N. C. Perkins and C. D. Mote Jr 1986 *Journal of Sound and Vibration* **106**, 451–463. Comments on curve veering in eigenvalue problems.


## APPENDIX A: TORSIONAL VIBRATION SOLUTION

The equation of motion of the shaft in Figure 1 while the system vibrates freely is [12]

$$\ddot{\varphi} = \tilde{c}^2 \varphi'', \tag{A.1}$$

where $\varphi$ is the rotating angle of any cross-section with respect to its free end, and the over dot symbol ( $\cdot$ ) and prime ( $'$ ) imply the derivations with respect to time $t$ and position co-ordinate $x$ respectively. Furthermore,

$$\tilde{c}^2 = \frac{G}{\rho_s}. \tag{A.2}$$

The associated boundary conditions (BC's) are

$$GI_s \varphi'(0, t) = 0, \qquad GI_s \varphi'(L_s,t) + J_D \ddot{\varphi}(L_s, t) = 0. \tag{A.3, 4}$$

Via separation of variables, a solution to equation (A.1) in the form $\varphi(x, t) = \Phi(x)\, T(t)$ is sought. It has been shown [12] that the functions $\Phi(x)$ and $T(t)$ are

$$\Phi(x) = A \cos \frac{\omega}{\tilde{c}} x + B \sin \frac{\omega}{\tilde{c}} x, \qquad T(t) = C \cos \omega t + D \sin \omega t\,, \tag{A.5, 6}$$

with $\omega$ being the circular frequency of free vibration. Boundary condition (A.3) yields $B = 0$. Substituting this result along with equations (A.5) and (A.6) into equation (A.4) yields the frequency equation of the system which is given by the relation

$$GI_s \left[ -A \frac{\omega}{\tilde{c}} \sin \frac{\omega}{\tilde{c}} L_s \right] - J_D \omega^2 A \cos \frac{\omega}{\tilde{c}} L_s = 0,$$

or after rearranging,

$$\tan \eta = -\frac{J_D}{J_s} \eta, \tag{A.7}$$

where $\lambda$ and $J_s$ are defined as

$$\eta = \frac{\omega}{\tilde{c}} L_s, \qquad J_s = \rho_s I_s L_s. \tag{A.8, 9}$$

Thus, equation (A.7) has countable infinite roots $\eta_1, \eta_2, \ldots$ .

Now, let us consider the special case where the shaft is represented by an effective lumped linear spring and the hub, beam, and payload are roughly approximated by a lumped rigid disk. Here, $k_t$ represents the equivalent torsional spring coefficient and is calculated as

$$k_t = \frac{GI_s}{L_s}. \tag{A.10}$$

The dish with the inertia $J_D$ is located at one end of the spring and the equivalent inertia of the shafts $J_s$ at the other end as it is the case in the models of many authors. Then, the natural frequency of this system is

$$\tilde{\omega} = \sqrt{\frac{J_s + J_D}{J_s J_D} k_t}, \tag{A.11}$$

where the tilde over $\omega$ indicates the discrete model approximation. Equation (A.11) can be transformed into the form

$$\frac{\tilde{\omega}}{\tilde{c}} L_s = \tilde{\eta} = \sqrt{(1 + \mu)}, \tag{A.12}$$

where $\tilde{\eta}$ again is an approximation to the exact $\eta$, if we define the ratio of mass moment of inertia as

$$\mu = \frac{J_s}{J_D}. \tag{A.13}$$

## APPENDIX B: CHARACTERISTIC EQUATION

The shaft performs torsional vibrations. As can be easily found from standard references (for example, reference [12]) its equation of motion is

$$\ddot{\varphi} = \tilde{c}^2 \varphi'', \tag{B.1}$$

The associated BCs are

$$GI_s\,\varphi'(0,\,t) = -\,T_d + J_R\,\ddot{\varphi}(0,\,t), \qquad GI_s\,\varphi'(L_s,t) = -\,T_r, \tag{B.2, 3}$$

where $J_R$, $T_d$ and $T_r$ are the rotor inertia, driving torque supplied by the motor, and resisting torque acting of the shaft due to the hub, respectively. The BC given by equation (B.3) can be rewritten in a more clear form by using the equation of motion of the hub. So applying Euler's equations to the hub yields

$$J_H\ddot{\varphi}\;\;(L_s,\,t) - T_r - M(0,\,t) + rV(0,\,t) = 0, \tag{B.4}$$

where $J_H$, $M$ and $V$ are the hub rotational inertia, and the applied bending moment and applied shear forces (the last two represent action on the hub by the root of the beam) respectively. Combining equations (B.3) and (B.4) yields

$$GI_s\,\varphi'(L_s,\,t) = -\,J_H\,\ddot{\varphi}\,(L_s,\,t) + M(0,\,t) - rV(0,\,t). \tag{B.5}$$

Now, let us confine our attention to a hub–beam–payload system as shown in Figure 2, where the parameters $L_B$, $A_B$, $I_B$, $\rho_B$, $E$, $r$, $M_P$ and $J_P$ all retain their meaning from section 4 of this paper. A dextral set of mutually perpendicular basis vectors $\hat{b}_1$, $\hat{b}_2$, $\hat{b}_3$, are fixed in the hub such that $\hat{b}_3$ is parallel to the axis of rotation of the hub, $\hat{b}_1$ is parallel to the centerline of the beam in its undeformed position, and $\hat{b}_2 = \hat{b}_3 \times \hat{b}_1$. A differential element of width d$s$ and mass

$$\mathrm{d}m = \rho_B A_B \mathrm{d}s \tag{B.6}$$

is located at a distance $s$ along the beam from its root by the position vector

$$\mathbf{r}^{dm} = x\hat{b}_1 + y\hat{b}_2. \tag{B.7}$$

The acceleration of this differential element with respect to the Newtonian reference frame $N$ is

$$\begin{aligned} {}^N\mathbf{a}^{dm} &= {}^N\mathbf{a}^o + {}^B\mathbf{a}^{dm} + {}^N\boldsymbol{\alpha}^B \times \mathbf{r}^{dm} + {}^N\boldsymbol{\omega}^B \times ({}^N\boldsymbol{\omega}^B \times \mathbf{r}^{dm}) + 2^N\,\boldsymbol{\omega}^B \times {}^B\mathbf{v}^{dm} \\ &= [\ddot{x} - y\ddot{\varphi} - \dot{\varphi}^2\,(r + x) - 2\dot{y}\dot{\varphi}]\,\hat{b}_1 + [\ddot{\varphi}(r + x) + \ddot{y} - \dot{\varphi}^2 y + 2\dot{x}\dot{\varphi}]\,\hat{b}_2, \end{aligned} \tag{B.8}$$

where $\dot{\varphi}$ and $\ddot{\varphi}$ are the angular velocity and angular acceleration, respectively, of the hub. The free-body diagram for this differential element is shown in Figure (B.1) where $M$, $V$, $T$ and $p$ represent the moment, shear load, tension in the beam, and the transverse applied loads, which are, respectively, acting on this element. The unit vectors $\hat{t}$ and $\hat{n}$ are local tangential and normal (transverse) directions associated with the centerline of the beam at this differential element. If we treat this as an Euler–Bernoulli beam, then summing the forces acting on this differential element in the $\hat{n}$ directions yields

$$\begin{aligned} \sum F_n &= p(s)\,\mathrm{d}s - \frac{\partial V}{\partial s}\,\mathrm{d}s - T\sin\theta + \left(T + \frac{\partial T}{\partial s}\,\mathrm{d}s\right)\sin\left(\theta + \frac{\partial \theta}{\partial s}\,\mathrm{d}s\right) \\ &\cong p(s)\,\mathrm{d}s - \frac{\partial V}{\partial s}\,\mathrm{d}s + T\left(\frac{\partial \theta}{\partial s}\right)\mathrm{d}s, \quad \text{where } \left(\theta \approx \frac{\partial y}{\partial s}\right) \\ &\cong p(s)\,\mathrm{d}s - \frac{\partial^2}{\partial s^2}\,(M)\,\mathrm{d}s + T\left(\frac{\partial^2 y}{\partial s^2}\right)\mathrm{d}s. \end{aligned} \tag{B.9}$$

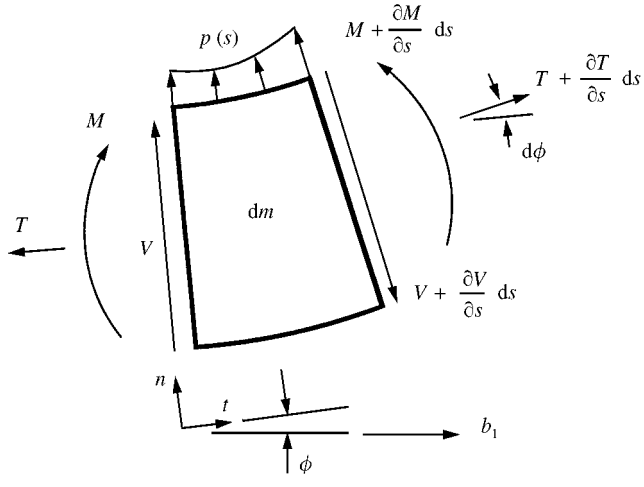


Figure B1. Free-body diagram of differential beam element.

The tension in the beam $T$ is given by

$$T \cong \int_x^{L_B} {}^N\mathbf{a}^{dm} \cdot \hat{b}_1 \, (\rho_B \, A_B \, \mathrm{d}x) + M_P \, {}^N\mathbf{a}^P \cdot \hat{b}_1$$

$$= \rho_B A_B \int_x^{L_B} (\ddot{x} - y\ddot{\varphi} - \dot{\varphi}^2 \, (r + x) - 2\dot{y}\dot{\varphi}) \, \mathrm{d}x + M_P \, [\ddot{x} - y\ddot{\varphi} - \dot{\varphi}^2 \, (r + x) - 2\dot{y}\dot{\varphi}] \, |_{L_B}$$

$$\cong \rho_B A_B \left\{ \ddot{\varphi}(t) \int_x^{L_B} y(x, t) \, \mathrm{d}x + 2\dot{\varphi}(t) \int_x^{L_B} \dot{y}(x, t) \, \mathrm{d}x + \dot{\varphi}(t) \, [\tfrac{1}{2} \, (L_B^2 - x^2) + r(L_B - x)] \right\}$$

$$+ M_P [\ddot{\varphi}(t) \, y(L_B, t) + \dot{\varphi}^2 (t) \, (r + L_B) + 2\dot{\varphi}(t) \, \dot{y}(L_B, t)]. \tag{B.10}$$

If we confine our attention to small deflections of an Euler–Bernoulli beam, then $\dot{x}$ and $\ddot{x}$ appearing in equation (B.10) may be neglected, also $\partial y/\partial x \approx \partial y/\partial s = \sin\theta, \cos\theta \approx 1$, and $\partial V/\partial s = M = EI_B \, \partial^2 y/\partial s^2$. Substituting these simplifications along with equations (B.7)–(B.10) into Newton's second law of motion, for the acceleration of the differential element in the $\hat{n}$ direction, yields

$$\sum F_n = (\rho_B \, A_B \, \mathrm{d}s) \, ({}^N\mathbf{a}^{dm} \cdot \hat{n})$$

or

$$p(s) - (EI_B y'')'' + \left[ \rho_B A_B \left\{ \ddot{\varphi} \int_x^{L_B} y \, \mathrm{d}x + 2\dot{\varphi} \int_x^{L_B} \dot{y} \, \mathrm{d}x + \dot{\varphi}^2 \, [\tfrac{1}{2} \, (L_B^2 - x^2) + r(L_B - x)] \right\} \right. \left. + M_P \, [\ddot{\varphi} \, y(L_B, t) + \dot{\varphi}^2 \, (r + L_B) + 2\dot{\varphi} \, \dot{y}(L_B, t)] \right] y''$$

$$= (\rho_B \, A_B) \, ([y\ddot{\varphi} + \dot{\varphi}^2 \, (r + x) + 2\dot{y}\dot{\varphi}] \, y' + [\ddot{\varphi}(r + x) + \ddot{y} - \dot{\varphi}^2 y]), \tag{B.11}$$

subject to the boundary conditions

$$y(0, t) = 0, \qquad y'(0, t) = 0, \tag{B.12, 13}$$

$$EI_B\, y''(L_B, t) = -J_P\, [\ddot{\varphi} + \ddot{y}'(L_B, t)], \tag{B.14}$$

$$EI_B\, y'''(L_B, t) = M_P\, [\ddot{\varphi}(r + L_B) + \ddot{y}(L_B, t) - \dot{\varphi}^2 y(L_B, t)]. \tag{B.15}$$

The first two BCs shown are of geometric character while the last two are the natural BCs.

Equations (B.1), (B.5), and (B.11), subject to the BCs (B.2), (B.12)–(B.15) form a coupled, highly non-linear set of differential equations. As such they pose no fundamental problems for purely numerical treatment. However, if one wishes to obtain estimates of the eigenvalues and eigenfunctions, which may in turn be used to improve the performance of a numerical treatment, then some simplifications are in order. Under the assumption of "small" deflections and "modest" hub rotations rates, we may reasonably neglect the $\dot{y}$, $\dot{\varphi}$, $y'$, and $y''$ terms appearing in equation (B.11), yielding

$$EI_B\, y^{\mathrm{IV}}(x, t) + \rho_B A_B\, \ddot{y}(x, t) = p(x, t) - \rho_B A_B (r + x)\, \ddot{\varphi}(L_s, t), \tag{B.16}$$

subject to the boundary conditions

$$y(0, t) = 0, \qquad y'(0, t) = 0, \tag{B.17, 18}$$

$$EI_B\, y''(L_B, t) = -J_P\, [\ddot{\varphi} + \ddot{y}'(L_B, t)], \tag{B.19}$$

$$EI_B\, y'''(L_B, t) = M_P\, [\ddot{\varphi}(r + L_B) + \ddot{y}(L_B, t)]. \tag{B.20}$$

Furthermore, if there is no forcing term $p(x, t)$, then the change of variable

$$\tilde{y}(x, t) = y(x, t) + (r + x)\, \varphi(L_s, t) \tag{B.21}$$

puts the equation of motion of the beam into a homogeneous form,

$$EI_B\, \tilde{y}^{\mathrm{IV}}(x, t) + \rho_B A_B\, \tilde{y}(x, t) = 0, \tag{B.22}$$

where $\tilde{y}$ physically represents the length of the arc tracked by any cross-section of the beam.

Solving equation (B.21) for $y$ and substituting its corresponding expression in terms of $\tilde{y}$ into equations (B.17)–(B.21) yields the equation of motion and associated BC's:

$$\tilde{y}(0, t) = r\varphi(L_s, t), \qquad \tilde{y}'(0, t) = \varphi(L_s, t), \tag{B.23, 24}$$

$$EI_B\, \tilde{y}''(L_B, t) = -J_P\, \ddot{\tilde{y}}'(L_B, t) \tag{B. 25}$$

and

$$EI_B\, \tilde{y}'''(L_B, t) = M_P\, \ddot{\tilde{y}}(L_B, t). \tag{B.26}$$

Similarly, from the Euler–Bernoulli bending hypothesis one can write the relationships

$$M(0, t) = EI_B\, y''(0, t) = EI_B\, \tilde{y}''(0, t), \tag{B.27}$$

$$V(0, t) = EI_B\, y'''(0, t) = EI_B\, \tilde{y}'''(0, t). \tag{B.28}$$

Substituting equations (B.27) and (B.28) into equation (B.5) gives

$$GI_s\, \varphi'(L_s, t) = -J_H \ddot{\varphi}(L_s, t) + EI_B\, \tilde{y}''(0, t) - r EI_B\, \tilde{y}'''(0, t). \tag{B.29}$$

If one applies the method of separation of variables to equations (B.1) and (B.22), which assumes the existence of solutions in the form of

$$\varphi(x, t) = \Phi(x)\ T(t), \qquad \tilde{y}(x, t) = Y(x)\ T(t), \tag{B.30, 31}$$

then after some tedious manipulations one obtains that the function $\Phi(x)$ and $Y(x)$ must be

$$\Phi(x) = A \cos \frac{\omega}{\tilde{c}}\, x + B \sin \frac{\omega}{\tilde{c}}\, x, \tag{B.32}$$

$$Y(x) = a \cosh \frac{\lambda}{L_B}\, x + b \cos \frac{\lambda}{L_B}\, x + c \sinh \frac{\lambda}{L_B}\, x + d \sin \frac{\lambda}{L_B}\, x \tag{B.33}$$

and

$$\lambda = \left[ \omega\ L_B^2 \sqrt{\frac{\rho_B A_B}{EI_B}} \right]^{1/2}. \tag{B.34}$$

Note that the $x$ variables in $\Phi(x)$ and $Y(x)$ are different, however the function $T(t)$ appearing in equations (B.30) and (B.31) must be same in each case because it represents the natural vibrations of the whole system, and has the form

$$T(t) = C \cos\omega t + D \sin \omega t, \tag{B.35}$$

where $\omega$ represents the natural frequency of the system. After substituting equations (B.32), (B.33) and (B.35), into equations (B.2), (B.3), (B.23)–(B.26) and performing the necessary manipulations one finds the following relationships:

$$J_R \omega^2\ A + GI_s \left( \frac{\omega}{\tilde{c}} \right) B = 0, \tag{B.36}$$

$$GI_s \left[ -\frac{\omega}{\tilde{c}} \sin \frac{\omega}{\tilde{c}}\, L_s\ A + \frac{\omega}{\tilde{c}} \cos \frac{\omega}{\tilde{c}}\, L_s B \right] = J_H \omega^2 \left[ \cos \frac{\omega}{\tilde{c}}\, L_s\ A + \sin \frac{\omega}{\tilde{c}}\, L_s B \right] + EI_B \left( \frac{\lambda}{L_B} \right)^2 \left[ a - b + r \left( \frac{\lambda}{L_B} \right) ( - c + d) \right], \tag{B.37}$$

$$a + b - r \left( A \cos \frac{\omega}{\tilde{c}}\, L_s\ A + B \sin \frac{\omega}{\tilde{c}}\, L_s \right) = 0, \tag{B.38}$$

$$\lambda(c + d) - L_B \left( A \cos \frac{\omega}{\tilde{c}}\, L_s\ + B \sin \frac{\omega}{\tilde{c}}\, L_s \right) = 0, \tag{B.39}$$

$$EI_B \left( \frac{\lambda}{L_B} \right) (a \cosh \lambda - b \cos \lambda + c \sinh\ \lambda - d \sin \lambda) = J_P \omega^2\ (a\ \sinh \lambda - b \sin \lambda + c \cosh \lambda \cdot c + d \cos \lambda), \tag{B.40}$$

$$EI_B \left( \frac{\lambda}{L} \right)^3 (a\ \sinh \lambda + b \sin \lambda + c \cosh\ \lambda - d \cos \lambda) = -\ M_P \omega^2\ (a \cosh \lambda + b \cos \lambda + c \sinh \lambda + d \sin \lambda). \tag{B.41}$$

Using the parameters given by equations (1)–(8) in the text, then equations (B.36)–(B.41) become

$$\alpha\lambda^4 A + \sqrt{\beta}\lambda^2 B = 0, \tag{B.42}$$

$$L_B\,[\lambda^2\,\sqrt{\beta}\sin(\sqrt{\beta}\lambda^2) + \lambda^4\gamma\cos(\sqrt{\beta}\lambda^2)]\;A + L_B\,[-\lambda^2\,\sqrt{\beta}\cos(\sqrt{\beta}\lambda^2) + \lambda^4\gamma\sin(\sqrt{\beta}\lambda^2)]B + R_b\lambda^2 a - R_b\lambda^2\;b - \bar{r}R_b\lambda^3 c + \bar{r}R_b\lambda^3 d = 0, \tag{B.43}$$

$$a + b - r\cos(\sqrt{\beta}\lambda^2)\;A - r\sin(\sqrt{\beta}\lambda^2)\;B = 0, \tag{B.44}$$

$$\lambda c + \lambda d - L_B\cos(\sqrt{\beta}\lambda^2)\;A - L_B\sin(\sqrt{\beta}\lambda^2)\;B = 0, \tag{B.45}$$

$$[\cosh\lambda - \lambda^3 R_e\sinh\lambda]\;a + [-\cos\lambda - \lambda^3 R_e\sin\lambda]\;b + [\sinh\lambda - \lambda^3 R_e\cosh\lambda]\,c + [-\sin\lambda + \lambda^3\;R_e\cos\lambda]\;d = 0, \tag{B.46}$$

$$[\sinh\lambda - \lambda R_f\cosh\lambda]\;a + [\sin\lambda + \lambda^3\;R_f\cos\lambda]\;b + [\cosh\lambda - \lambda^3 R_f\sinh\lambda]\,c + [-\cos\lambda - \lambda^3\;R_f\sin\lambda]\;d = 0. \tag{B.47}$$

Equations (B.42)–(B.47) produce a set of six homogeneous equations which is linear in the six unknowns $A$, $B$, $a$, $b$, $c$, $d$. Because this is a homogeneous set of equations, the determinant of the coefficients' matrix must be zero in order that this system of equations have non-trivial solutions. Hence, the $\lambda$ values, which make the following determinant zero are the eigenvalues (associated with the eigenfrequencies) of the system:

$$\begin{vmatrix} 0 & 0 & 0 & 0 & a\lambda^4 & \sqrt{\beta}\lambda^2 \\ R_b\lambda^2 & -R_b\lambda^2 & -\bar{r}R_b\lambda^3 & \bar{r}R_b\lambda^3 & L_B[\lambda^2\sqrt{\beta}\sin(\sqrt{\beta}\lambda^2) + \lambda^4\gamma\cos(\sqrt{\beta}\lambda^2)] & L_B[-\lambda^2\sqrt{\beta}\cos(\sqrt{\beta}\lambda^2) + \lambda^4\gamma\sin(\sqrt{\beta}\lambda^2)] \\ 1 & 1 & 0 & 0 & -r\cos(\sqrt{\beta}\lambda^2) & -r\sin(\sqrt{\beta}\lambda^2) \\ 0 & 0 & \lambda & \lambda & -L_B\cos(\sqrt{\beta}\lambda^2) & -L_B\sin(\sqrt{\beta}\lambda^2) \\ (\cosh\lambda - \lambda^3 R_e\sinh\lambda) & (-\cos\lambda + \lambda^3 R_e\sin\lambda) & (\sinh\lambda - \lambda^3 R_e\cosh\lambda) & (-\sin\lambda - \lambda^3 R_e\cos\lambda) & 0 & 0 \\ (\sinh\lambda + \lambda R_f\cosh\lambda) & (\sin\lambda + \lambda R_f\cos\lambda) & (\cosh\lambda + \lambda R_f\sinh\lambda) & (-\cos\lambda + \lambda R_f\sin\lambda) & 0 & 0 \end{vmatrix} = 0. \tag{B.48}$$

It can be easily seen that the determinant will be zero for $\lambda = 0$. This is expected because the system is semi-definite. Equation (B.48) is the characteristic equation for the system whose roots are the eigenvalues (or natural frequencies) of the system. Its expansion is not given here due to its complexity. However, the determinant given by equation (B.48) can be expanded by using any symbolic mathematical code (like Maple or Mathematica), as has been done in this study.

## APPENDIX C: NOMENCLATURE

For this investigation, the symbols which are important to the development of system equations of motion and associated boundary conditions are

| | |
|---|---|
| $A_B$ | cross-sectional area of beam (manipulator arm) |
| $A_S$ | cross-sectional area of shaft |
| $\hat{b}_1, \hat{b}_2, \hat{b}_3$ | dextral orthogonal basis vectors fixed in hub |
| $\tilde{c}$ | wave propagation velocity of torsional wave in shaft |
| $E$ | Young's modulus of beam material |
| $G$ | shear modulus of shaft (effective driveline) material |
| $I_B$ | area moment of inertia of *beam* |
| $I_s$ | area moment of inertia of *shaft* |
| $J_B$ | rigid-body mass moment of inertia of *beam* about its root end |
| $J_D$ | mass moment of inertia for lumped *disk* crudely representing rotor–beam–payload system |
| $J_H$ | mass moment of inertia of the *hub* which connects the beam to the shaft |
| $J_P$ | effective mass moment of inertia of *payload* (end effector + work piece) |
| $J_R$ | effective mass moment of inertia of *rotor* (motor armature, etc.) |
| $J_s$ | rigid-body mass moment of inertia of the *shaft* |
| $L_B$ | length of *beam* |
| $L_s$ | effective length of *shaft* |
| $M$ | bending moment acting on differential element of beam |
| $M_B$ | total mass of *beam* |
| $M_P$ | mass of *payload* (end effector + work piece) |
| $\hat{n}$ | unit vector normal to centerline of beam at differential element, lying in plane of motion |
| $p$ | transverse distributed lad applied to beam |
| $r$ | radius of hub |
| $\bar{r}$ | dimensionless length |
| $R_a$ | rotational inertia ratio of beam to rotor |
| $R_b$ | stiffness ratio of beam to shaft |
| $R_c$ | rotational inertia ratio between beam and shaft |
| $R_d$ | rotational inertia ratio of beam to hub |
| $R_e$ | rotational inertia ratio between payload and beam |
| $R_f$ | mass ratio of payload to the beam |
| $s$ | arc length along beam locating differential element |
| $t$ | time |
| $\hat{t}$ | unit vector parallel to centerline of beam of differential element |
| $T$ | tension in beam |
| $T_d$ | driving torque supplied by motor |
| $T_r$ | resisting torque felt by shaft |
| $V$ | transverse shear acting on differential element of beam |
| $x$ | local radial co-ordinate associated with location as defined by $s$ |
| $y$ | local transverse co-ordinate associated with location as defined by $s$ |
| $\tilde{y}$ | local transverse co-ordinate which implicitly considers shaft twist. |
| $\alpha$ | scaled ratio of $R_b$ to $R_a$ |
| $\beta$ | scaled ratio of $R_b$ to $R_c$ |
| $\gamma$ | scaled ratio of $R_b$ to $R_d$ |
| $\rho_B$ | mass density of *beam* material |
| $\rho_s$ | mass density of *shaft* |
| $\lambda$ | system eigenvalue |
| $\phi$ | rotation of shaft |
| $\theta$ | local rotation of differential element of beam due to deformation of beam |
| $\omega$ | natural circular frequency of system |
| $\eta$ | beam eigenvalue |